Desalination and Water Treatment
www.deswater.com

doi: 10.5004/dwt.2018.21919

104 (2018) 206–216
February

Simultaneous removal of Na, Ca, K and Mg from synthetic brine and seawater using Fe_2O_3–SiO_2 mixed oxide nanostructures: kinetics and isotherms studies

Denga Ramutshatsha, J. Catherine Ngila, Patrick G. Ndungu, Philiswa N. Nomngongo*

Department of Applied Chemistry, University of Johannesburg, Doornfontein Campus, P.O. Box 17011, Johannesburg 2028, South Africa, Tel. +27115596187; emails: pnnomngongo@uj.ac.za, nomngongo@yahoo.com (P.N. Nomngongo), denga.makhwedzha18@gmail.com (D. Ramutshatsha), jcngila@uj.ac.za (J.C. Ngila), pndungu@uj.ac.za (P.G. Ndungu)

Received 13 July 2017; Accepted 10 January 2018

ABSTRACT

In the study, Fe_2O_3–SiO_2 nanocomposite (prepared using sol–gel method), was used as an adsorbent for the removal of Na, K, Ca and Mg ions from synthetic brine solutions. The structural and surface characteristics of the nanoadsorbent were investigated by N_2 adsorption–desorption, transmission electron microscopy, scanning electron microscopy coupled with energy dispersive X-ray spectroscopy and powder X-ray diffraction spectroscopy. The batch adsorption technique was used for removal of major cations from the synthetic samples. Experimental parameters (such as pH, initial concentration, adsorbent mass and contact time) affecting the removal of Na, K, Ca and Mg were optimized using response surface methodology. Equilibrium isotherms for the simultaneous adsorption of Na, K, Ca and Mg onto Fe_2O_3–SiO_2 nanocomposite were analyzed by the Freundlich, Langmuir, Dubinin–Radushkevich (D–R) and Temkin isotherm models. Adsorption isotherm studies indicate that the simultaneous adsorption of Na, K, Ca and Mg ions onto Fe_2O_3–SiO_2 nanocomposite followed models in the order Langmuir > Temkin ≈ Dubinin–Radushkevich (D–R) > Freundlich model. The kinetic study of adsorption shows that the batch adsorption system followed pseudo-second-order kinetic model. The isotherm and kinetic studies confirmed that the adsorption of major cations was based on physical adsorption mechanism.

Keywords: Major elements, Fe_2O_3–SiO_2 nanocomposite; Isotherms; Adsorption kinetic; Adsorption desalination

1. Introduction

Concentrated brine is generated in desalination plant in high level and they cause environmental problem [1,2]. The World Health Organization (WHO) guideline for permissible limit of salinity in drinking water is 500 mg L^{-1} and in some special cases it goes up to 1,000 mg L^{-1}. The brine produced often has a total dissolved solids concentration of between 20,000 and 35,000 mg L^{-1} [3]. Several technologies and potential technologies for desalination have been studied [4–7]. Distillation and membrane are the major desalination processes. While minor processes such as direct solar desalination are suitable for remote areas with expected low income [8]. Distillation systems are more energy intensive (up to four times more) than reverse osmosis systems, but require less pretreatment of the water and are therefore generally considered to be more robust. However, in countries such as South Africa, thermal desalination processes might not be considered for desalination of brackish or seawater, unless sufficient waste heat or low cost fuels are available [9]. The current methods that have been developed from traditional methods include the desalination of water by surfactant [10], capacitive deionization [11], microbial desalination [12] and forward osmosis [13]. Most of these desalination methods remove ions from the water in a non-selective because they also include the removal of important nutrients. Ziolkowska [14] reported that desalination costs are increasing for all desalination technologies and difficult to project the future developments of desalination due to market fluctuation [14].

* Corresponding author.

1944-3994/1944-3986 © 2018 Desalination Publications. All rights reserved.

For this reason, adsorption desalination (AD) has been developed as one of the possible alternatives to the conventional desalination systems [15].

Adsorption processes have been widely used for heating, cooling, sea or brackish desalination and wastewater treatment [16–18]. Operation of AD cycle is batch operated. The performance of AD cycle depends on how the adsorbents behave in equilibrium adsorption isotherms and kinetics. As a result, large adsorbents with surface area and large pore network for molecule transport are needed. Desalination studies have been done on materials such as graphene sheet [19] and zeolite [20], among others. In order to improve removal efficiencies and adsorption capacities, chemical modifications of low-cost adsorbents have to be investigated. Magnetic iron oxide nanoparticles have been identified as a suitable material due to their chemical stability in aqueous environment and low cost [21]. For this reason, magnetic iron oxide nanoparticles have been widely used in water treatments due to their potential adsorbents for removal of metallic ions and possible surface modification to improve their efficiency. In addition, their magnetic properties allow the separation of the adsorbent from solution by applying the external magnetic field [22]. However, the drawbacks of using pure iron oxide nanoparticles include rapid oxidation and aggregation in solution. As a result, these limitations reduce the adsorption capacity of the magnetic nanoparticle [23]. To overcome these challenges silica nanoparticles have been incorporated on the magnetic cores to enhance their chemical stability and surface area [23].

The optimization of parameters affecting the removal of major elements in a batch adsorption methodology has been performed using univariate technique (means, monitoring one factor at time [OFAT]). However, the disadvantage of the OFAT is that the interaction effects among the parameter are not considered. In addition, the consumption of reagent and materials increases and it is time consuming [24]. This can be solved by applying multivariate tools such as response surface methodology (RSM). This is because RSM is able to provide optimal conditions for desired responses and allows the evaluation of interaction of factors that may influence treatment efficiency [25]. Application of RSM for the optimization of on batch processes has been reported on the literature [26–28].

The main aim of this study is to evaluate the possibility of using nanomaterials as an adsorbent for the removal of Na, Ca, K and Mg in synthetic brine solutions and real seawater. Various parameters affecting sorption process such as pH, adsorbent dose, initial concentration (IC) and contact time (CT) were investigated using RSM. In addition, the kinetic models, that is, pseudo-first-order, pseudo-second-order and intraparticle diffusion were examined. Finally, various isotherm models such as Freundlich, Langmuir, Dubinin–Radushkevich and Temkin were used to identify the best-fit isotherm equation.

2. Experimental

2.1. Material

Tetraethyl orthosilicate (TEOS), hydrochloric acid (HCl), ammonium hydroxide (NH_4OH; 25%, w/v) and ferric nitrate ($Fe(NO_3)_3{\cdot}9H_2O$) were purchased from Sigma-Aldrich (St Louis, USA). Sodium nitrite ($NaNO_3$), magnesium sulfate ($MgSO_4$) and potassium nitrate (KNO_3) were obtained from Associated Chemical Enterprises (Johannesburg, South Africa). The calcium sulfate ($CaSO_4$) obtained from LabChem, Zelienople, Pennsylvania. The required concentration of Na^+, K^+, Ca^{2+} and Mg^{2+} was prepared from a 2,000 mg L^{-1} stock solution by making appropriate dilutions using ultrapure water. The pH of the solution was adjusted to desired value using dilute solutions of HCl or NH_3.

2.2. Instrumentation

An oven (EcoTherm, LaboTec, Midrand, South Africa) was used as drying source for the synthesized of the material. The iCAP 6500 Duo inductively coupled plasma atomic emission spectroscopy (ICP-OES; Thermo Scientific, UK) was used for quantification of major elements. The ICP-OES parameters during analysis were as follows: RF generator power (W): 1,150, frequency of RF generator (MHz): 40, coolant gas flow rate(L min^{-1}): 12, carrier gas flow rate (L min^{-1}): 0.7, auxiliary gas (L min^{-1}): 1, pump rate (rpm): 50, viewing configuration/touch mode: radial at a replicate: 3 and flush time (s): 30.

The phase formation and crystallographic state of all the samples were studied by X-ray diffraction (XRD) analysis using PANalytical X'Pert X-ray Diffractometer, and Cu Kα radiation spectrometer and the scanning area covered the range 2θ at start position 4.00–80.00 and a scan step time of 196.2 s. The morphology of the catalyst was studied by scanning electron microscopy (SEM; Hitachi COM-S-4200). The Si/Fe ratio was also determined by energy dispersive X-ray (EDX) spectroscopy which is connected to SEM. Fourier-transform infrared (FTIR) spectra were recorded on a PerkinElmer (BX 12) spectrophotometer using KBr pellets. Nitrogen adsorption–desorption isotherms were obtained at 77 K using Brunauer–Emmett–Teller (BET) micromeritics ASAP 2020. The BET equation was used to obtain the specific surface area and pore size distribution.

2.3. Synthesis of Fe_2O_3–SiO_2 by sol–gel method

The synthesis of Fe_2O_3–SiO_2 was adopted from the literature with some modifications [29]. For the synthesis of Fe_2O_3–SiO_2 nanocomposite, 60 mL of deionized water was mixed with 76 mL of absolute ethanol and stirred for 15 min. The 4.7 g of TEOS (98%) was added to the resulting solution and vigorously stirred for 30 min. Then, 0.92 g of $Fe(NO_3)_3{\cdot}9H_2O$ (Si/Fe = 50, respectively) was added at once and stirred for 30 min during which color of the solution changes to light yellow. For gel formation, 23 mL of 30% ammonium hydroxide was added and the gel formed was stirred for another 30 min and aged for 24 h at room temperature. The material was then dried for a day in an oven at 60°C for 24 h and calcined at 550°C for 4 h in a furnace.

2.4. Isotherm studies

Langmuir, Freundlich, Dubinin–Radushkevich (D-R) and Temkin model were used in this study to establish the relationship between the amount of adsorbed Na, K, Ca and Mg onto Fe_2O_3–SiO_2 and its equilibrium concentration. Langmuir

isotherm is used to describe a homogeneous monolayer chemical adsorption process [30]. Langmuir isotherm can be arranged in its linear form as the following:

$$\frac{C_e}{q_e} = \frac{1}{q_{\max}} C_e + \frac{1}{K_L q_{\max}} \tag{1}$$

where C_e is the equilibrium concentration of the studied metal (mg L^{-1}) and q_e is the amount of the metal adsorbed per gram of adsorbent (mg g^{-1}). The $q_{\max}$ and K_L are Langmuir constant relating the adsorption capacity (mg g^{-1}) and energy of adsorption (L g^{-1}) [30]. These constants can be calculated from the slopes of linear plots C_e/q_e vs. C_e, respectively. The important characteristic of Langmuir isotherm can be expressed in terms of dimensionless constant factor R_L. The equation of R_L is written as follows:

$$R_L = \frac{1}{1 + bC_o} \tag{2}$$

where C_o (mg L^{-1}) is IC of adsorbate and b (L mg^{-1}) is Langmuir constant. The four possibilities for adsorption are as follows: (i) favorable adsorption if $0 < R_L < 1$, (ii) unfavorable adsorption when $R_L > 1$, (iii) linear adsorption for $R_L = 1$ and also (iv) irreversible adsorption for $R_L = 0$ [31,32].

The Freundlich isotherm can be used for non-ideal sorption that involves heterogeneous surface energy system and multilayer sorption [33]. The linear equation for Freundlich is as follows:

$$\ln q_e = \ln K_F + \frac{1}{n} \ln C_e \tag{3}$$

where K_F is the Freundlich constant which relates to adsorption capacity and n is the Freundlich exponent, determined from the intercept and slope of linear plot of $\ln q_e$ vs. $\ln C_e$. In order to determine the type of sorption whether chemical or physical, equilibrium data were also applied to the Dubinin–Radushkevich (D–R) model [34,35]. The linear form of D–R isotherm is presented in the following equation:

$$\ln q_e = \ln q_{\mathrm{DR}} - \beta\varepsilon^2 \tag{4}$$

where q_e is the amount of metal ions adsorbed onto per unit dosage of Fe_2O_3–SiO_2 (mol g^{-1}), q_{DR} is the theoretical monolayer sorption capacity (mol g^{-1}), β is the constant of the sorption energy (mol^2 J^{-2}) and ε is the Polanyi potential ($\varepsilon = RT\ln\left(1 + \frac{1}{C_e}\right)$), where R is the gas constant (8.314 J mol^{-1} K^{-1}) and T is the temperature (K).

The E value ranges from 1 to 8 kJ mol^{-1} for physical sorption and from 8 to 16 kJ mol^{-1} for chemical sorption [36]. The mean free energy of adsorption (E, J mol^{-1}) estimates the type of sorption process and is calculated using Eq. (5):

$$E = \frac{1}{\sqrt{-2\beta}} \tag{5}$$

Temkin isotherm considered the effects of some indirect adsorbate/adsorbate interaction on adsorption isotherms it also suggests that the heat of adsorption of all the molecules in the layer would decrease linearly with coverage because of the interactions [37].

Temkin isotherm can be linearized as follows:

$$q_e = B_1 \ln K_T + B_1 \ln C_e \tag{6}$$

where $B = RT/b$, b is the Temkin constant related to heat of sorption (J mol^{-1}), A is the Temkin isotherm constant (L g^{-1}), R is the gas constant (8.314 J mol^{-1} K^{-1}) and T is the absolute temperature (K).

2.5. Adsorption studies

Equilibrium adsorption studies on removal of Na, K, Ca and Mg metals on saline water were conducted on a batch experiment from water samples of ICs of 25–1,000 mg L^{-1}. In these experiments, 20 mL of Na^+, K^+, Ca^{2+} and Mg^{2+} solution contained in 100 mL plastic bottles were contacted with 0.1–1.0 g of Fe_2O_3–SiO_2. The adsorption capacity (q_e, mg g^{-1}) was calculated using Eq. (7):

$$q_e = \frac{(C_o - C_e)V}{m} \tag{7}$$

where C_o (mg L^{-1}) is the IC of cations in saline water solution and C_e (mg L^{-1}) is equilibrium concentration of metal ions in water after treatment. V is the volume of the solution (L), m is the mass of the adsorbent used (g) and q_e (mg g^{-1}) is the amount of Na^+, K^+, Ca^{2+} and Mg^{2+} adsorbed at equilibrium.

2.6. Adsorption kinetics

The pseudo-first-order, pseudo-second-order and the intraparticle diffusion models were applied to the experimental data to examine adsorption process. The equation for pseudo-first-order can be written as follows:

$$\ln(q_e - q_t) = \ln q_e - k_1 t \tag{8}$$

where q_t is the amount of adsorbate, adsorbed (mg g^{-1}) at time t, k_1 is the rate constant (min^{-1}). The first-order rate constant can be calculated from the intercept and slope of the plot [38]. Pseudo-second-order equation is as follows:

$$\frac{t}{q_t} = \frac{1}{k_2 q_e^2} + \frac{1}{q_e} t \tag{9}$$

where the equilibrium sorption capacity (q_e) and the second-order constant k_2 (g mg^{-1} min^{-1}) (Table 4) can be determined experimentally from the slope and intercept of plot of t/qt vs. t. In addition, the initial sorption rate (h) and the half-adsorption times were calculated from Eqs. (10) and (11):

$$h = k_2 q_e^2 \tag{10}$$

$$t_{1/2} = \frac{1}{k_2 q_e} \quad (11)$$

In intraparticle diffusion model adsorbate species are most probably transported from the bulk of the solution into the solid phase through intraparticle diffusion, whereby is evaluated by the relationship between the time–dependent and adsorption capacity (q_t) and $t^{1/2}$. The intraparticle diffusion equation is as follows:

$$q_t = k_d t^{1/2} + c \quad (12)$$

where k_d is the intraparticle diffusion rate constant (mg g^{-1} min$^{-1/2}$) and c is the intercept.

2.7. Analysis of real seawater samples

Natural seawater samples collected from Durban, South Africa, were used to evaluate the applicability of the optimized desalination method. Seawater samples were collected in polyethylene bottles and pH and conductivity were measured. Detailed data analysis of the seawater using ICP-OES revealed that the samples contained about 10,403–10,793, 384–401, 395–401 and 1,293–1,341 mg L^{-1} of Na, K, Ca and Mg, respectively; the pH and conductivity were found to be 8.3 and 4.77 × 10^5 μS. Batch adsorption experiments of raw seawater samples without any previous treatments were performed optimum conditions.

3. Results and discussion

3.1. Characterization

The morphologies of SiO_2, Fe_2O_3 and Fe_2O_3–SiO_2 composite were studied by SEM/EDX and the micrographs obtained for these materials are shown in Figs. 1(a)–(c). As observed by SEM, Fig. 1(a) shows silica particles with irregular shapes that looks like polygonal. Fig. 1(b) shows details of the prepared iron oxide nanoparticles. The Fe_2O_3–SiO_2 composite (Fig. 1(c)) showing porous morphological structure which suggests that the nanocomposite could be a good adsorbent.

Fig. 2(a) shows SEM–EDS of prepared SiO_2, Fe_2O_3 and Fe_2O_3–SiO_2 composite. The prepared SiO_2 material (Fig. 2(a)) shows the weight percentage of 78.5% Si and 21.5% O. Fig. 2(b) shows that the Fe_2O_3 material was composed of O, Fe and C, respectively, with the weight percentage given as 36.7%, 34.5% and 28.8%, respectively. The EDS peaks on Fe_2O_3–SiO_2 composite demonstrate confirmed the presence of Fe, Si, O and C, and the carbon peak that can be observed from EDS spectrum (Figs. 2(a) and (b)) originated from the carbon coating.

The XRD pattern of SiO_2, Fe_2O_3 and synthesized Fe_2O_3–SiO_2 nanocomposites are shown in Fig. 3. Fig. 3(a) shows the amorphous state of SiO_2 with a broad peak at 2θ angles 15.00° and 40.00°. Fig. 3(b) shows crystalline peaks for Fe_2O_3 appeared at 2θ angles of 43.4°, 49.22°, 53.5°, 57.40° and 74.6°. The composite material Fe_2O_3–SiO_2 at Fig. 3(c) had crystalline structure at 2θ values 35.3°, 44.73°, 56.1° and 63.8° corresponding to Fe_2O_3. The broad peak at 2θ 15.0° and 30.0° (Fig. 3(c)) indicates the presence of SiO_2. This XRD spectrum is in agreement with the one obtained by Panda et al. [29].

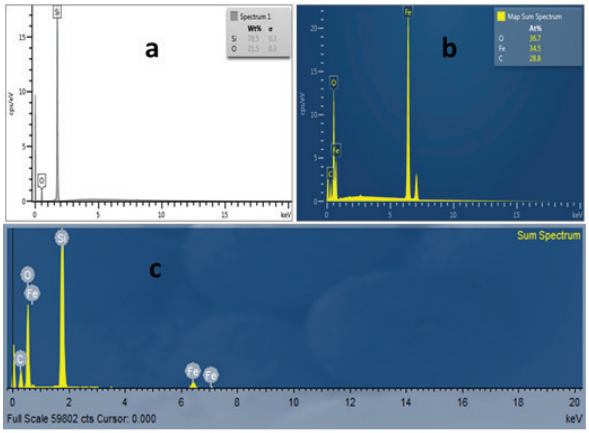

Fig. 2. (a) SEM–EDS image of (a) SiO_2, (b) Fe_2O_3 and (c) Fe_2O_3–SiO_2.

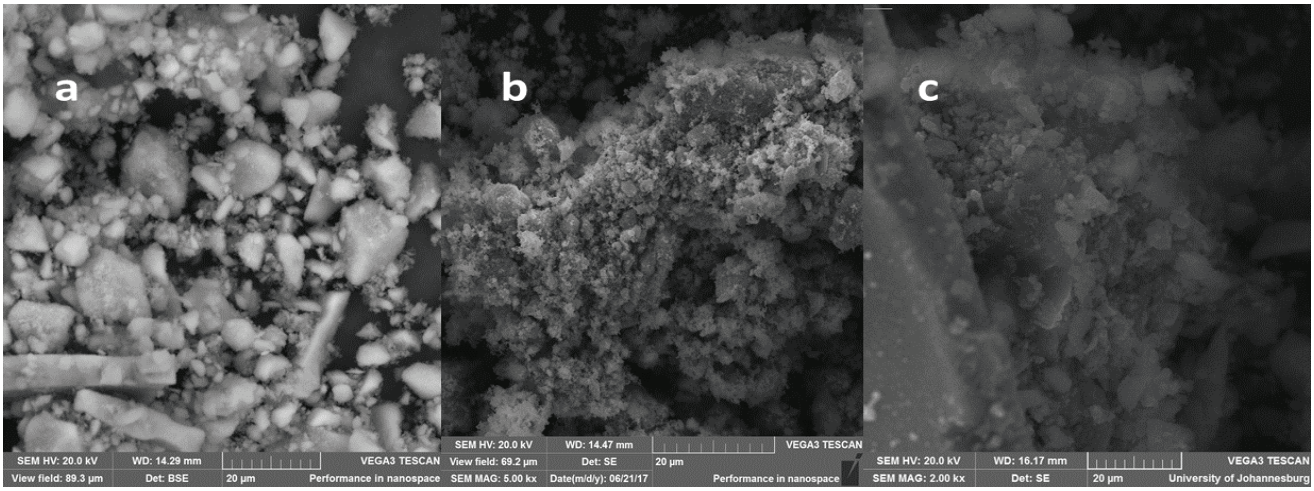

Fig. 1. (a) SEM image of (a) SiO_2, (b) Fe_2O_3 and (c) Fe_2O_3–SiO_2.

Fig. 4 shows the transmission electron microscopy (TEM) images of Fe_2O_3 and synthesized Fe_2O_3–SiO_2 composite. The iron oxide image (Fig. 4(a)) has been dominated by spherical shapes with very few cubic and hexagonal shapes, whereas Fe_2O_3–SiO_2 composites (Fig. 4(b)) only show the appearance of structures like hexagonal in shape.

3.2. N_2 adsorption and desorption isotherm study

The adsorption and desorption isotherms of nitrogen on SiO_2 and Fe_2O_3–SiO_2 composite at 77 K. Adsorption isotherms of the composite present features which can be described as type-IV according to IUPAC classification [39], which are typical characteristics of mesoporous materials. The surface

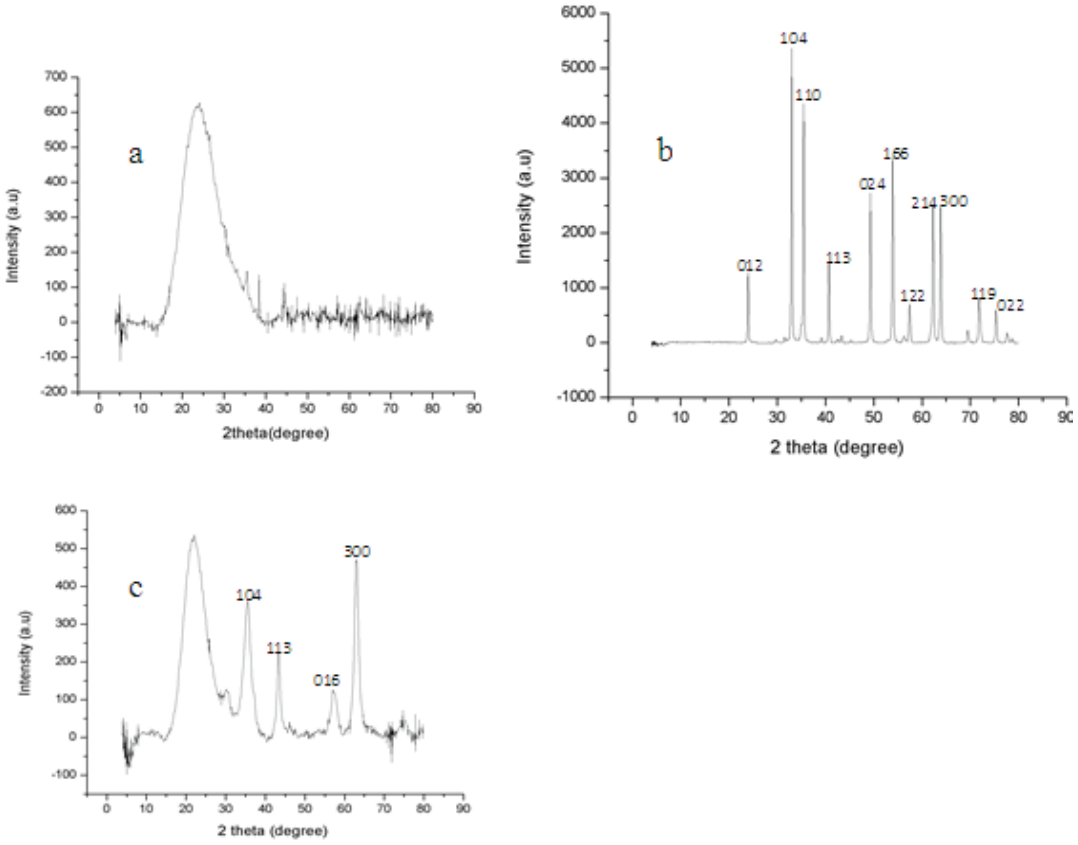

Fig. 3. (a) XRD patterns of (a) SiO_2, (b) Fe_2O_3 and (c) Fe_2O_3–SiO_2.

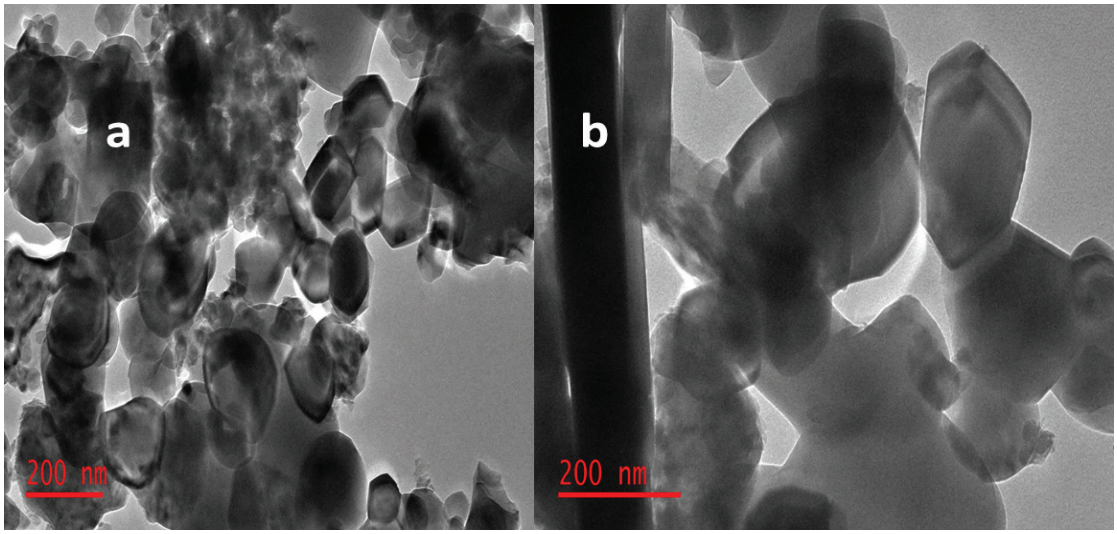

Fig. 4. (a) TEM image of (a) Fe_2O_3 and (b) Fe_2O_3–SiO_2.

area of SiO_2, Fe_2O_3 and Fe_2O_3–SiO_2 was found to be 265, 6.79 and 253 $m^2 g^{-1}$, respectively. The reduced surface area of the composite material from 295 to 253 $m^2 g^{-1}$ might be due to the introduction of iron oxide.

3.3. Optimization using response surface methodology on removal of Na, K, Ca and Mg ions onto Fe_2O_3–SiO_2 nanocomposite

The experimental parameters (sample pH, CT, IC and adsorbent mass [MA]) affecting the simultaneous removal of metal ions was optimized using multivariate statistical technique. The central composite design (CCD) matrix and analytical results for each run that were performed as per the experimental design are tabulated in Table 1. To assess the significance of the main effects and their interactions, the experimental results were statistically analyzed by means of analysis of variance that is presented in a form of Pareto chart (Fig. 5).

The IC and the interaction between MA and IC (2 L by 3 L) were found to be significant at 95% confidence level. These results implied that interaction of IC and MA together with IC were responsible in quantitative removal of metals Na^+, K^+, Ca^{2+} and Mg^{2+} in synthetic brine solution. For this reason, the response surface model was used to calculate the optimum conditions of pH, MA, CT and IC.

In order to investigate the interactive effect of two independent factors and their interactions on the amount of the major cations adsorbed at equilibrium, the response surface plots were constructed using the quadratic models of the RSM. Fig. 6 shows the 3D plot for the combined effect of MA with pH of the solution, IC and CT on adsorption equilibrium. The combined effect of IC with MA (Fig. 6(b)) shows that maximum adsorption capacity was achieved at MA of 0.5–1 g and IC of 800–1,000 mg L^{-1}. Effect of CT with MA on adsorption capacity can be seen in Fig. 6(c). The graph shows that when MA was 0.1 g and CT of 16–25 min high adsorption capacity of 120 mg g^{-1} and above was obtained. The results obtained in Fig. 6 are in agreement with the results shown in Fig. 5 by Pareto chart.

The optimum values obtained from the following factors that are sample pH, extraction time, IC and mass of adsorbent were obtained by checking the maxima formed by the *X* and *Y* coordinates [23,30]. The optimum conditions for removal of Na, K, Ca and Mg were found to be pH 7.5, 15 min, 1,000 mg L^{-1} and 1.0 g for sample pH, extraction time, IC and mass of adsorbent, respectively.

Table 1
Central composite design matrix and analytical response

Runs	pH	MA	IC	CT	Adsorption equilibrium (Q_e)			
					Ca	K	Mg	Na
1	9	1	1,000	5.0	17.8	33.3	10.4	16.5
2	9	1	25	5.0	0.42	0.76	0.25	0.36
3	9	0.1	1,000	30.0	183	319	104	155
4	2	1	25	30.0	0.42	0.64	0.23	0.28
5	9	0.1	25	30.0	4.23	9.05	2.48	3.63
6	2	0.1	1,000	5.0	193	339	116	161
7	2	1	1,000	30.0	19.4	34.2	11.7	16.3
8	2	0.1	25	5.0	4.19	6.15	2.26	3.23
9	2	0.55	512	17.5	18.0	27.0	10.0	12.9
10	9	0.55	512	17.5	18.8	33.3	10.6	15.7
11	5.5	0.1	512	17.5	101	151	52.1	72.5
12	5.5	1	512	17.5	10.1	15.4	5.24	7.27
13	5.5	0.55	25	17.5	0.58	0.86	0.49	0.54
14	5.5	0.55	1,000	17.5	35.9	64.1	20.6	29.7
15	5.5	0.55	512	5.0	18.5	27.54	9.57	13.2
16	5.5	0.55	512	30.0	18.5	27.11	9.51	12.9
17	5.5	0.55	512	17.5	18.6	27.56	9.61	13.1
18	5.5	0.55	512	17.5	18.5	27.19	9.56	12.9

MA = adsorbent mass, IC = initial concentration, and CT = contact time.

3.4. Confirmation experiments

The confirmatory experiments were performed in order to validate the analytical data given by RSM model under optimized conditioned. The results obtained from the RSM predicted that response for sorption of metal ion Ca, K, Mg and Na ranged from 90% to 93%. The percentage removal efficiency was used to assess the performance of adsorbent on each metal ion. The experiments were conducted under the parameters suggested by the model (pH 7.5, adsorbent dose 0.1 g, IC 1,000 mg L^{-1} and extraction time 16 min). Results show that the synthesized Fe_2O_3–SiO_2 composite to remove Ca, K, Mg and Na metal ions from saline water in the range of 93%–95% which is a close range predicted by the RSM model.

3.5. Equilibrium adsorption isotherm studies

The equilibrium adsorption data were fitted to the isotherm models such as Langmuir, Freundlich, Temkin and Dubinin–Radushkevich. Under optimum conditions, the isotherm experiments were carried out at 298 with 25–1,000 mg L^{-1} concentrations. The regression correlation coefficient (R^2) values were used as a measure of the goodness of fit of experimental data on the models and the isotherm parameters are

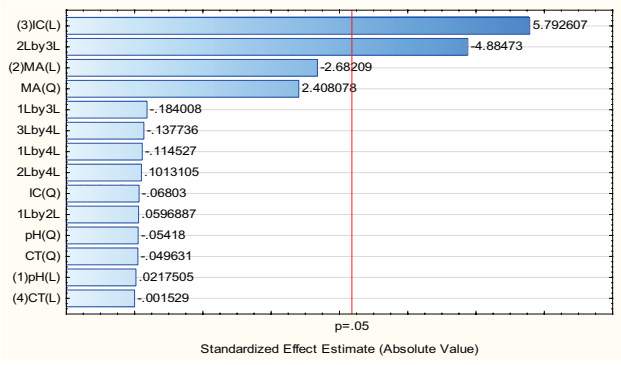

Fig. 5. Pareto chart of standardized estimated effects caused by the factors investigated.

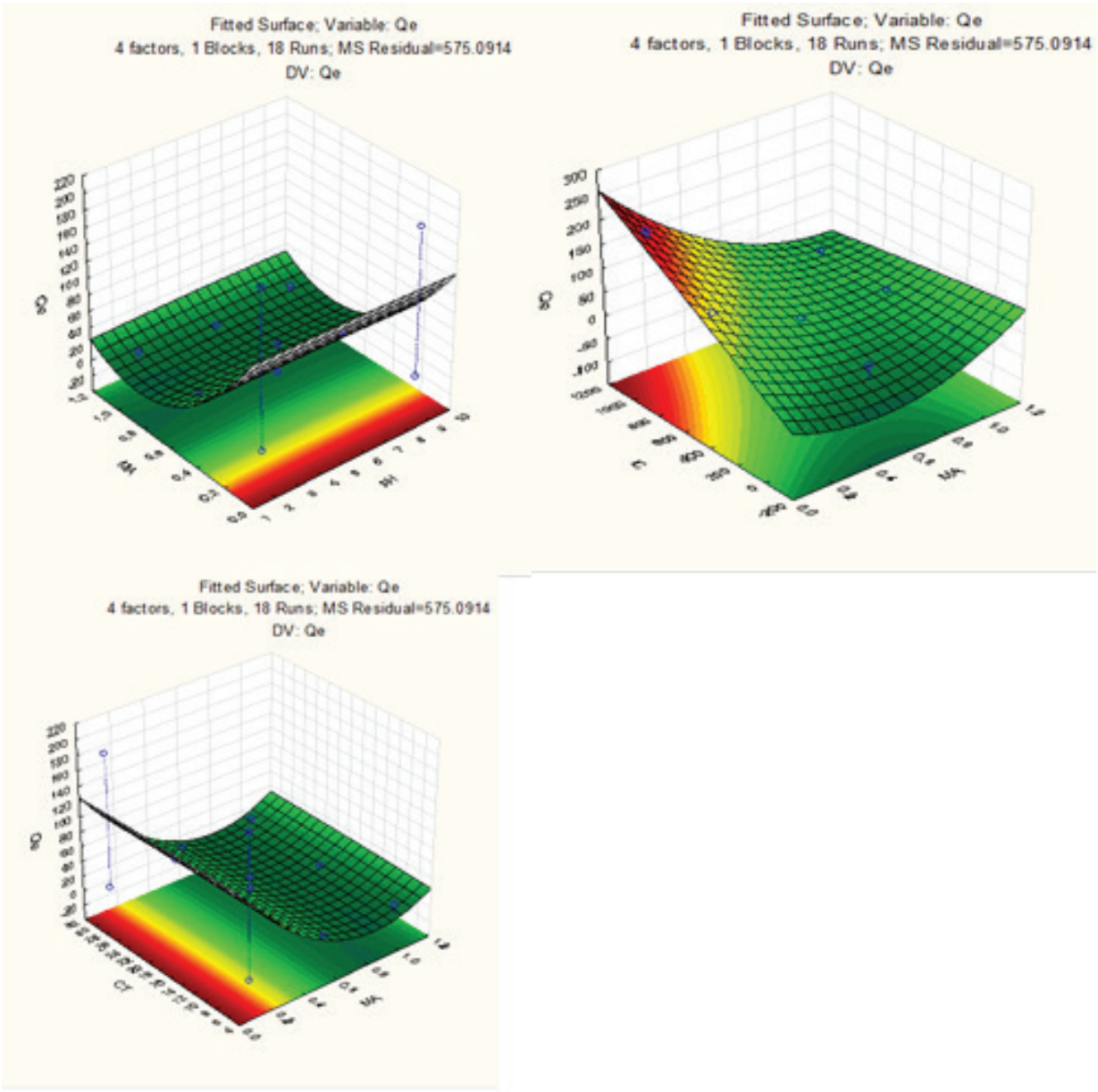

Fig. 6. Response surface plot showing the combined effect of adsorbent mass with pH and initial concentration on adsorption capacity: other factors were fixed at central point.

summarized in Tables 2 and 3. It should be noted that the R^2 values are >0.99, indicated a very good mathematical fit. It can be seen from Tables 3 and 4 that the order of fitting of the studied isotherms was Langmuir > Temkin ≈ Dubinin–Radushkevich (D–R) > Freundlich model for all the major cations. The Langmuir isotherm model suggests that the uptake occurs on a homogenous surface by monolayer sorption and all the sorption sites are energetically identical [30]. The maximum adsorption capacity of the nanoadsorbent according to the Langmuir isotherm (q_{max}) was calculated to be 152, 164, 161 and 181 mg g^{-1} for Ca, K, Mg and Na, respectively.

The analysis of Langmuir model and affinity between the major cations and the adsorbent were further predicted using the Langmuir parameter b from the dimensionless constant separation factor R_L, which is defined in section 2.4. The calculated R_L values for adsorption of Ca, K, Mg and Na onto the surface of the adsorbent were found to be 0.04, 0.06, 0.08 and 0.08, respectively. These results suggested that the Fe_2O_3–SiO_2 adsorbent is highly favorable for adsorption of Na^+, K^+, Ca^{2+} and Mg^{2+} ions from synthetic brine solution under the optimum conditions used in this study.

The D–R isotherm model was used to determine the nature of physical or chemical adsorption processes [34,35] the nature of adsorption mechanism was estimated using the mean free energy of adsorption (E, kJ mol^{-1}) and the results are presented in Table 3. It can be seen that the adsorption mean free energy for the removal of Ca, K, Na and Mg was less than 8 kJ mol^{-1} (Table 3). These results indicated that the mechanisms of adsorption of the major cations onto the nanoadsorbents were physical sorption.

In this study, the Temkin adsorption isotherm model was used to evaluate the adsorption potentials of Fe_2O_3–SiO_2 adsorbent/metal ion interactions and the parameters are presented in Table 4. These results suggested that in adsorption processes using the nanoadsorbent, sorbent/metal ion interactions were effective for all major cations.

3.6. Adsorption kinetics

In this study, the kinetics models were used to assess the mechanism of adsorption and its potential rate-determining steps, which include mass transport and chemical reaction processes [32]. Moreover, the information obtained on the kinetics of major cation uptake will be used to select the conditions that can be used for a full-scale AD processes. Lagergren pseudo-first-order and pseudo-second-order kinetic models as well as intraparticle diffusion were used to assess mechanism of adsorption and its potential rate-determining steps.

The results of the pseudo-first-order, pseudo-second-order and intraparticle diffusion calculated using their respective model equations are summarized in Table 4. The suitability of each kinetic model was judged using the correlation coefficient (R^2) and the agreement between experimental and calculated q_e values [32]. Based on correlation coefficients (R^2), the pseudo-second-order model ($R^2 \geq 0.99$) gives the best fitting for sorption of Na, K, Ca and Mg onto Fe_2O_3–SiO_2, compared with the pseudo-first-order model ($R^2 \leq 0.7$). In addition, the calculated q_e values were in good agreement with the experimental values. The agreement between the experimental and calculated values of pseudo-second-order model maximum sorption capacities (q_e) for Fe_2O_3–SiO_2 validates the applicability of Na, K, Ca and Mg sorption.

Table 2
Adsorption isotherms constant values for Freundlich and Langmuir

Langmuir parameters				
Cations	$Q_{max,exp}$	q_{max} (mg g^{-1})	K_L (L mg^{-1})	R^2
Ca	151	152	0.67	0.9999
K	163	164	0.45	0.9997
Mg	160	161	0.47	0.9999
Na	178	182	0.37	0.9995
Freundlich parameters				
		K_F	n	R^2
Ca		1.4	5	0.6887
K		1.3	3	0.7725
Mg		1.3	3	0.7054
Na		1.4	3	0.7523

Table 3
Adsorption isotherms constant values for Dubinin–Radushkevich and Temkin model

Dubinin–Radushkevich (D–R)				
Cations	q_{DR} (mol g^{-1})	β × 10^{-7} (mol^2 J^{-2})	E (kJ mol^{-1})	R^2
Ca	142	–2.3	1.47	0.8788
K	114	–1.5	1.83	0.8959
Mg	120	–2.0	1.58	0.8942
Na	137	–3.0	1.29	0.8504
	Temkin parameters			
	K_T (L g^{-1})	B	R^2	
Ca	21.8	19.0	0.8360	
K	11.0	23.4	0.8977	
Mg	12.0	22.7	0.8871	
Na	8.74	29.8	0.8908	

Table 4
Pseudo-first-order, pseudo-second-order and intraparticle diffusion for sorption of Na, K, Mg and Ca

		Ca	K	Mg	Na
Pseudo-first-order	q_e exp	151	163	160	178
	k_1 (min^{-1})	0.0838	0.0683	0.0497	0.0538
	q_e (mg g^{-1})	24.6	40.0	20.6	45.5
	R^2	0.7610	0.5962	0.4962	0.5953
Pseudo-second-order	k_1 (g mg^{-1} min^{-1})	0.003	0.009	0.002	0.001
	q_e (mg g^{-1})	153	163	162	181
	R^2	0.9969	0.9989	0.9913	0.9893
	h (mg g^{-1} min^{-1})	75.2	25.5	57.5	35.3
	$t_{1/2}$ (min)	2.04	6.43	2.81	5.15
Intraparticle diffusion	k_{id1} (g mg^{-1} min^{-1})	65.9	88.9	81.5	94.2
	C_1 (mg g^{-1})	46.9	154	108	144
	R_1^2	0.9959	0.9650	0.9872	0.9808
	k_{id1} (g mg^{-1} min^{-1})	0.294	0.0921	0.0873	0.566
	C_2 (mg g^{-1})	149	161	161	174
	R_2^2	0.386	0.493	0.53	0.54

Therefore, the adsorption mechanism was classified as the second-order nature of the adsorption process. Similar to Langmuir isotherm model, pseudo-second-order kinetics assumes that the rate-limiting step may be chemisorption involving valence forces through sharing and exchange of electrons [32,40–42].

Pseudo-second-order kinetic rate constant (k_2) and adsorption capacity (q_e) were further used to calculate the initial sorption rate (h), and the half-adsorption time ($t_{1/2}$) and the results are presented in Table 4. Half-adsorption time refers to the time required to remove half of the amount of the analyte of interest at equilibrium [32] and is considered as a measure of the adsorption rate [32]. The results obtained revealed that there was relatively high affinity between the adsorbent and metal ions. This is because half-adsorption times for all metal ions were short (ranging 2–6 min). In addition, the initial sorption rate for all the studied major cations was in the order Ca > Mg > Na > K.

The sorption kinetic data were further analyzed to understand the role of intraparticle diffusion on the entire adsorption process. In addition, intraparticle diffusion was used to further identify the steps of adsorption process. The kinetic data were fitted on multilinear plots of intraparticle diffusion process for the sorption of major cations onto the surface of nanoadsorbent demonstrated that two steps took place. According to the literature, the two steps correspond to film diffusion which is the diffusion of analyte molecules from solution to the external surface of the adsorbent, and intraparticle diffusion, that is, the diffusion of analyte molecules through pores of the nanoadsorbent [41]. In addition, the multilinear plots did not pass through the origin, suggesting the intraparticle diffusion is not the rate-limiting step [41]. This suggested that some other mechanisms also play an important role in the adsorption of major elements.

The constant values for intraparticle diffusion (k_{id}) and C were calculated from the intercept and slope and the parameters and R^2 are presented in Table 4. It can be seen that k_{id1} is larger than k_{id2}. This observation suggested that the film diffusion process was rapid compared with the intraparticle diffusion which was a gradual process [43]. In addition, the correlation coefficients indicated a good applicability of intraparticle diffusion model in assessing the steps that take place during the adsorption of major elements onto the surface of SiO_2–Fe_2O_3 nanoadsorbent [43].

3.7. Reusability and regeneration studies

Regeneration/reusability property of an adsorbent is one the important aspect in adsorption-based studies for a cost-effective metal ion removal process. Under optimum conditions, the adsorption–desorption cycles repeated 10 times were carried out using synthetic seawater samples (containing 1,000 mg L^{-1} for each analyte). To remove the adsorbed cations, the spent adsorbent was treated with 2.0 mol L^{-1} HNO_3, sonicated for 1 h, and filtered. After filtration, the filtrate was analyzed using ICP-OES. The removal efficiency of the adsorbent remained constant for seven cycles (Table 5). This suggested the prepared nanocomposite was relatively stable and can be reusable.

3.8. Application to real samples

The applicability of Fe_2O_3–SiO_2 nanocomposite to remove Ca, K, Mg and Na from real seawater was investigated. The analytical results before adsorption and percentage removal are presented in Table 6. The results obtained indicated that Fe_2O_3–SiO_2 is suitable for the removal of major elements (percentage removal efficiency ranged from 83% to 98%) from seawater. In addition, considering the high ICs especially Na and Mg, Fe_2O_3–SiO_2 nanocomposite exhibited high potential as adsorbent that can be used in desalination real seawater or brines. For this reason, future studies will investigate the adsorptive removal of Na, K, Mg and Ca in real seawater using continuous column system.

The comparison of Fe_2O_3–SiO_2 nanocomposite with other carbon-based materials reported previously in the literature for removal of major cation is shown in Table 7. It can be seen from this table that the performance of the current material is comparable or even better than some carbon-based materials [44–47].

4. Conclusion

The Fe_2O_3–SiO_2 nanocomposite as an adsorbent was prepared using sol–gel method and characterized by XRD,

Table 5
Adsorption–desorption studies

Cycles	Cation % removal efficiency			
	Ca	K	Mg	Na
1	98.1 ± 2.1	99.3 ± 1.1	99.2 ± 2.3	99.6 ± 2.1
3	98.2 ± 2.3	99.1 ± 1.8	99.3 ± 0.8	99.1 ± 0.9
5	98.0 ± 1.9	99.6 ± 2.0	98.8 ± 1.0	98.2 ± 1.0
7	96.8 ± 2.5	96.7 ± 1.3	97.9 ± 1.6	96.7 ± 1.2
10	88.3 ± 3.1	85.4 ± 2.8	82.9 ± 1.9	88.9 ± 3.8

Table 6
Application of Fe_2O_3–SiO_2 nanocomposite for removal of major elements in real samples

Analytes	Initial concentration (mg L^{-1})	Removal efficiency (%)	Initial concentration (mg L^{-1})	Removal efficiency (%)
	Sample 1		Sample 2	
Na	10,403 ± 42	83.7 ± 1.2	10,793 ± 70	81.2 ± 1.7
K	384 ± 10	98.2 ± 1.4	401 ± 9	98.6 ± 2.3
Ca	401 ± 6	98.0 ± 1.5	395 ± 9	97.9 ± 1.3
Mg	1,293 ± 15	90.2 ± 2.3	1,341 ± 15	89.5 ± 2.3

Table 7
Comparison with carbon-based adsorbents

Analytes	Adsorbent	Removal efficiency (%)	Reference
Na, Mg	Activated carbon	80, 72	[44]
Ca, Mg, Na	Fe_3O_4-MWNTs	73, 67, 70	[45]
Na, Mg, Ca, K	Functionalized graphene sheets	68, 71, 60, 56	[46]
Mg, Na	f-MWNTs	88, 72	[47]
Ca, K, Mg, Na	Fe_2O_3–SiO_2	98, 98.7, 90, 84	This work

FTIR, SEM, TEM, BET and EDX techniques. The parameters affecting the experimental parameters for removal of Ca, K, Mg and Na in synthetic saline samples were optimized using RSM based on CCD. Under optimized condition, the adsorption followed Langmuir model better than Freundlich isotherm. The maximum adsorption capacity was 152, 164, 161 and 181 mg g^{-1} for Ca, K, Mg and Na, respectively. The value of R_L from Langmuir isotherm indicates that the sorption of Na^+, K^+, Ca^{2+} and Mg^{2+} ions was favorable. While the mean free energy of adsorption was <8 kJ mol^{-1} suggesting the mechanisms of adsorption of the major cations onto the nanoadsorbents were physisorption. In addition, the adsorption of the major elements followed second-order kinetics as well as film and intraparticle diffusion mechanisms. Moreover, the results obtained indicated that Fe_2O_3–SiO_2 nanocomposite could be a potential adsorbent for the AD process.

Acknowledgments

The authors would like to thank the DAAD/NRF joint in-country scholarships and NRF Thuthuka (grant no. 99270) for their financial assistance and the University of Johannesburg (UJ), for providing their laboratory facilities.

References

[1] T. Younos, Environmental issues of desalination, J. Contemp. Water Res. Educ., 132 (2005) 11–18.
[2] A.S. Sánchez, I.B.R. Nogueira, R.A. Kalid, Uses of the reject brine from inland desalination for fish farming, *Spirulina* cultivation, and irrigation of forage shrub and crops, Desalination, 364 (2015) 96–107.
[3] P. Dama-Fakir, A. Toerien, Evaporation Rates on Brine Produced During Membrane Treatment of Mine Water, International Mine Water Conference, Pretoria, South Africa, 2009, pp. 19–23.
[4] J.W. Wu, M.J. Biggs, E.J. Hu, Dynamic model for the optimization of adsorption-based desalination processes, Appl. Therm. Eng., 66 (2014) 464–473.
[5] K. Thu, B.B. Saha, K.J. Chua, K.C. Ng, Performance investigation of a waste heat-driven 3-bed 2-evaporator adsorption cycle for cooling and desalination, Int. J. Heat Mass Transfer, 101 (2016) 1111–1122.
[6] J.S. Ho, Z. Ma, J. Qin, S.H. Sim, C.S. Toh, Inline coagulation–ultrafiltration as the pretreatment for reverse osmosis brine treatment and recovery, Desalination, 365 (2015) 242–249.
[7] M. Naimi, C. Innocent, D.E. Akretche, Chloride behavior in electromembrane treatment of brine issued from desalination plants, J. Appl. Electrochem., 40 (2010) 1079–1083.
[8] M.M.A. Rayan, B. Djebedjian, Advances in Desalination Technologies: Solar Desalination, Potable Water, Springer International Publication, Switzerland, 2014, pp. 181–211.
[9] J.A. du Plessis, A.J. Burger, C.D. Swartz, N. Musee, A Desalination Guide for South African Municipal Engineers, WRC Report No. TT 266/06, Water Research Commission, Pretoria, South Africa, 2006.
[10] M.B. Zenouz, Desalination water with surfactant a new method with clear vision, Nat. Sci., 42 (2009) 86.
[11] I. Cohen, E. Avraham, A. Soffer, D. Aurbach, Water desalination by capacitive deionization-advantages limitations and modification, ECS Trans., 45 (2013) 43–59.
[12] X. Cao, X. Huang, P. Liang, K. Xiao, Y. Zhou, X. Zhang, B.E. Logan, A new method for water desalination using microbial desalination cells, Environ. Sci. Technol., 43 (2009) 7148–7152.
[13] H. Li, L. Zou, Ion-exchange membrane capacitive deionization: a new strategy for brackish water desalination, Desalination, 275 (2011) 62–66.
[14] J.R. Ziolkowska, Is desalination affordable?—Regional cost and price analysis, Water Resour. Manage., 29 (2015) 1385–1397.
[15] A.S. Alsaman, A.A. Askalany, K. Harby, M.S. Ahmed, A state of the art of hybrid adsorption desalination–cooling systems, Renew. Sustain. Energy Rev., 58 (2016) 692–703.
[16] N. Ghaffour, T.M. Missimer, G.L. Amy, Technical review and evaluation of the economics of water desalination: current and future challenges for better water supply sustainability, Desalination, 309 (2013) 197–207.
[17] K.C. Ng, K. Thu, Y. Kim, A. Chakraborty, G. Amy, Adsorption desalination: an emerging low-cost thermal desalination method, Desalination, 308 (2013) 161–179.
[18] M.R. Awual, Ring size dependent crown ether based mesoporous adsorbent for high cesium adsorption from wastewater, Chem. Eng. J., 303 (2016) 539–546.
[19] Y. You, V. Sahajwalla, M. Yoshimura, R.K. Joshi, Graphene and graphene oxide for desalination, Nanoscale, 8 (2016) 117–119.
[20] S. Jeong, H. Chung, T. Yoon, S. Lee, Scalants removal from synthetic RO brine using natural zeolite, J. Korean Soc. Water Wastewater, 30 (2016) 279–284.
[21] F. Le Formal, M. Grätzel, K. Sivula, Controlling photoactivity in ultrathin hematite films for solar water-splitting, Adv. Funct. Mater., 20 (2010) 1099–1107.
[22] E. Ghasemi, A. Heydari, M. Sillanpää, Superparamagnetic Fe_3O_4@EDTA nanoparticles as an efficient adsorbent for simultaneous removal of Ag(I), Hg(II), Mn(II), Zn(II), Pb(II) and Cd(II) from water and soil environmental samples, Microchem. J., 131 (2017) 51–56.
[23] S. Bao, K. Li, P. Ning, J. Peng, X. Jin, L. Tanga, Highly effective removal of mercury and lead ions from wastewater by mercaptoamine-functionalised silica-coated magnetic nano-adsorbents: behaviors and mechanisms, Appl. Surf. Sci., 393 (2017) 457–466.
[24] M.A. Bezerra, R.E. Santelli, E.P. Oliveira, L.S. Villar, L.A. Escaleira, Response surface methodology (RSM) as a tool for optimization in analytical chemistry, Talanta, 76 (2008) 965–977.
[25] A.L. Ahmad, S.S. Wong, T.T. Teng, A. Zuhairi, Optimization of coagulation–flocculation process for pulp and paper mill effluent by response surface methodological analysis, J. Hazard. Mater., 145 (2007) 162–168.
[26] F. Ghorbani, H. Younesi, S.M. Ghasempouri, A.A. Zinatizadeh, M. Amini, A. Daneshi, Application of response surface methodology for optimization of cadmium biosorption in an aqueous solution by *Saccharomyces cerevisiae*, Chem. Eng. J., 145 (2008) 267–275.
[27] L.V.A. Reddy, Y.J. Wee, J.S. Yun, H.W. Ryu, Optimization of alkaline protease production by batch culture of *Bacillus* sp. RKY3 through Plackett–Burman and response surface methodological approaches, Bioresour. Technol., 99 (2008) 2242–2249.
[28] C. Chellamboli, M. Perumalsamy, Application of response surface methodology for optimization of growth and lipids in *Scenedesmus abundans* using batch culture system, RSC Adv., 4 (2014) 22129–22140.
[29] N. Panda, H. Sahoo, S. Mohapatra, Decolourization of methyl orange using Fenton-like mesoporous Fe_2O_3–SiO_2 composite, J. Hazard. Mater., 185 (2011) 359–365.
[30] I. Langmuir, The adsorption of gases on plane surfaces of glass, mica and platinum, J. Am. Chem. Soc., 40 (1918) 1361–1403.

[31] K.G. Bhattacharyya, A. Sarma, Adsorption characteristics of the dye, Brilliant Green, on Neem leaf powder, Dyes Pigm., 7 (2003) 211–222.
[32] P.N. Nomngongo, J.C. Ngila, T.A. Msagati, B. Moodley, Kinetics and equilibrium studies for the removal of cobalt, manganese, and silver in ethanol using Dowex 50W-x8 cation exchange resin, Sep. Sci. Technol., 49 (2014) 1848–1859.
[33] H.M.F. Freundlich, Über die adsorption in lösungen, Z. Phys. Chem., 57 (1906) 385–470.
[34] H. Zheng, D. Liu, Y. Zheng, S. Liang, Z. Liu, Sorption isotherm and kinetic modeling of aniline on Cr-bentonite, J. Hazard. Mater., 167 (2009) 141–147.
[35] M.A. Zenasni, S. Benfarhi, A. Merlin, S. Molina, B. George, B. Meroufel, Adsorption of Cu(II) on maghnite from aqueous solution: effects of pH, initial concentration, interaction time and temperature, Nat. Sci., 4 (2012) 856.
[36] H. Zheng, Y. Wang, Y. Zheng, H. Zhang, S. Liang, M. Long, Equilibrium, kinetic and thermodynamic studies on the sorption of 4-hydroxyphenol on Cr-bentonite, Chem. Eng. J., 143 (2008) 117–123.
[37] M.J. Temkin, V. Pyzhev, Recent modifications to Langmuir isotherms, Acta Physiochim. URSS, 12 (1940) 217–222.
[38] S. Lagergren, Zur theorie der sogenannten adsorption geloster stoffe, K. Sven. Vetensk.akad. Handl., 24 (1898) 1–39.
[39] M. Thommes, K. Kaneko, A.V. Neimark, J.P. Olivier, F. Rodriguez-Reinoso, J. Rouquerol, K.S. Sing, Physisorption of gases, with special reference to the evaluation of surface area and pore size distribution (IUPAC Technical Report), Pure Appl. Chem., 87 (2015) 1051–1069.
[40] F. Ghomri, A. Lahsini, A. Laajeb, A. Addaou, The removal of heavy metal ions (copper, zinc, nickel and cobalt) by natural bentonite, Larhyss J., 12 (2013) 37–54. ISSN 1112-3680.
[41] K.Z. Setshedi, M. Bhaumik, S. Songwane, M.S. Onyango, A. Maity, Exfoliated polypyrrole-organically modified montmorillonite clay nanocomposite as a potential adsorbent for Cr(VI) removal, Chem. Eng. J., 222 (2013) 186–197.
[42] M. Sadeghi, M. Irandoust, F. Khorshidi, M. Feyzi, F. Jafari, T. Shojaeimehr, M. Shamsipur, Removal of Arsenic (III) from natural contaminated water using magnetic nanocomposite: kinetics and isotherm studies, J. Iran. Chem. Soc., 13 (2016) 1175–1188.
[43] Z. Chen, J. Zhang, J. Fu, M. Wang, X. Wang, R., Han, Q. Xu, Adsorption of methylene blue onto poly (cyclotriphosphazene-co-4, 4′-sulfonyldiphenol) nanotubes: kinetics, isotherm and thermodynamics analysis, J. Hazard. Mater., 273 (2014) 263–271.
[44] E. Hettiarachchi, R. Perera, A.D.L. Chandani Perera, N. Kottegoda, Activated coconut coir for removal of sodium and magnesium ions from saline water, Desal. Wat. Treat., 57 (2016) 22341–22352.
[45] A.K. Mishra, S. Ramaprabhu, Magnetite decorated multiwalled carbon nanotube based supercapacitor for arsenic removal and desalination of seawater, J. Phys. Chem. C, 114 (2010) 2583–2590.
[46] A.K. Mishra, S. Ramaprabhu, Functionalized graphene sheets for arsenic removal and desalination of sea water, Desalination, 282 (2011) 39–45.
[47] A.K. Mishra, S. Ramaprabhu, The role of functionalised multiwalled carbon nanotubes based supercapacitor for arsenic removal and desalination of sea water, J. Exp. Nanosci., 7 (2012) 85–97.